Int. J. Multiphase Flow, Vol. 3, pp. 67–77. Pergamon/Elsevier, 1976. Printed in Great Britain.

THE BEHAVIOUR OF LARGE DROPS IN IMMISCIBLE LIQUIDS

T. WAIREGI† and J. R. GRACE

Department of Chemical Engineering, McGill University, P.O. Box 6070, Montreal, Quebec, Canada H3C 3G1

(*Received* 10 *April* 1975)

Abstract—The motion of large drops with Eötvos numbers as high as 1000 has been investigated in large tanks where wall effects are negligible. Shapes observed include ellipsoidal- and spherical-caps with and without skirts, crescents, biconcave disks, toroids and wobbling irregular forms. The ellipsoidal-cap drops are shown to obey an equation based upon an extension of the Davies and Taylor theory for bubbles in liquids, regardless of whether skirts are being formed and shed at the rear.

INTRODUCTION

Extensive work has been performed on the mechanics of small and medium size bubbles and drops. Large gas bubbles have also received considerable attention in the literature. However, there has been very little work on large drops, drops for which the Eötvos number, $Eo = gd_e^2\Delta\rho/\sigma$, is greater than about 40 where g is the acceleration of gravity, d_e the volume-equivalent sphere diameter, σ the interfacial or surface tension and $\Delta\rho = |\rho_c - \rho_d|$ the absolute value of the density difference between the continuous and dispersed phases. The present paper presents experimental data regarding such liquid drops rising or falling in an immiscible liquid media of large extent. Drops up to a litre in volume were injected; the systems studied covered a broad range of physical properties with the modified M-group, $M = \Delta\rho g\mu_c^4/\rho_c^2\sigma^3$, covering the range 5.7×10^{-12} to 2.4×10^3. Here μ_c is the continuous phase viscosity. For the drops described in the present paper, the Eötvos number ranged between about 10 and 1000.

EXPERIMENTAL APPARATUS AND PROCEDURE

Most of the experiments were carried out in a large tank of 1.22 m^2 cross-section and of depth 2.44 m. This tank consisted of Plexiglass windows held in place by a rigid cast iron framework. With such a large tank, wall effects were negligible, even for the large drops studied here. In view of the large volume of liquid required to fill this tank, its use was restricted to water and aqueous sugar solutions as continuous phase liquids. Experiments wherein ethylene glycol and paraffin oil were used as the continuous phase were carried out in a cylindrical glass column of diameter 0.46 m and height 2.8 m.

Before measurements were taken, the dispersed liquid to be used was stirred with an equal weight of the continuous fluid. Fluid densities were then determined with a calibrated hydrometer or using a conventional weighing method by means of a pycnometer. Liquid viscosities were measured over a range of temperature from 18 to 40°C using Brookfield rotational and Cannon–Fenske capillary viscoemeters. Interfacial tensions were determined using a ring tensiomat. Temperatures were measured prior to each run and ranged between 24 and 30°C. The physical properties for all systems and values of the modified M-group are presented in table 1. No stringent measures were taken to eliminate all surface active agents from the liquids used.

Single drops (or bubbles) were formed by injecting the desired volume into an inverted semi-circular cup near the base of the column. The drop was released by rotating the cup into an upright position using a bimba air cylinder. Immediately after release, the drop passed through

†Present address: Domtar Reserch Centre, Senneville, Québec, Canada.

Table 1. Systems studied and physical properties

System No.	Dispersed phase	Continuous phase	Density ρ_c (g/cm^3)	Density ρ_d (g/cm^3)	Viscosity μ_c, P	Viscosity μ_d, P	Interfacial tension σ (dyn/cm)	M-group	Temperature (°C)
1	Chloroform	Aq. Sugar solution	1.39	1.483	30.8	0.0056	32.7	1.2×10^{3}	19.0
2	Carbon tetrachloride	Aq. Sugar solution	1.38	1.586	30.8	0.0105	34.4	2.3×10^{3}	19.2
3	5 cS silicone oil	Aq. Sugar solution	1.39	0.92	28.9	0.055	53.5	1.1×10^{3}	19.5
4	Carbon tetrachloride	Aq. Sugar solution	1.39	1.586	12.0	0.0104	34.4	5.1×10^{1}	27.3
5	Air	Aq. Sugar solution	1.366	0.00126	3.4	0.00018	76.2	2.2×10^{-1}	27.0
6	Chloroform	Aq. Sugar solution	1.366	1.483	3.0	0.0056	25.2	3.1×10^{-1}	28.5
7	50 cS silicone oil	Aq. Sugar solution	1.366	0.958	3.1	0.465	27.1	9.9×10^{-1}	28.0
8	Air	Aq. Sugar solution	1.392	0.00126	13.35	0.00018	79.1	4.5×10^{1}	28.5
9	50 cs silicone oil	Aq. Sugar solution	1.31	0.958	0.54	0.465	24.6	1.1×10^{0}	25.0
10	Chloroform	Aq. Sugar solution	1.31	1.483	0.54	0.0056	31.4	2.7×10^{-4}	25.0
11	Air	Paraffin oil	0.883	0.00126	2.0	0.00018	37.5	3.4×10^{-1}	19.5
12	1,2-Dichloroethane	Ethylene glycol	1.112	1.247	0.148	0.0104	6.9	1.5×10^{-4}	22.0
13	Air	Aq. Sugar solution	1.30	0.00126	0.37	0.00018	73.6	3.5×10^{-5}	19.5
14	Air	Ethylene glycol	1.112	0.00126	0.135	0.00018	42.0	4.0×10^{-6}	25.0
15	50 cS silicone oil	Water	0.998	0.948	0.010	0.465	44.2	5.7×10^{-12}	19.6
16	Water	Paraffin oil	0.883	0.998	1.1	0.010	52.7	1.4×10^{-3}	25.0
17	50 cS silicone oil	Ethylene glycol	1.112	0.958	0.124	0.465	24.0	2.1×10^{-6}	23.5
18	Glycerine	Paraffin oil	0.883	1.272	1.85	12.5	38.8	9.8×10^{-2}	17.0
19	50 cS silicone oil	Paraffin oil	0.883	0.958	2.0	0.465	7.0	4.4×10^{0}	20.0
20	o-Dichlorobenzene	Aq. Sugar solution	1.38	1.288	11.2	0.0137	36.8	1.5×10^{1}	27.8
21	o-Diethyl Phthalate	Aq. Sugar solution	1.38	1.115	11.2	0.0890	29.4	8.5×10^{1}	27.8
22	5 cS silicone oil	Aq. Sugar solution	1.38	0.92	11.6	0.0545	53.5	2.8×10^{1}	26.5

an open control gate, operated by a second bimba air cylinder, which could be closed to trap any satellites following the principal drop or bubble. In cases where the dispersed liquid was more dense than the continuous liquid, drops were released manually by pouring from above. Best results were achieved by gently immersing the cup before tipping it to release its contents.

The motion of rising and falling fluid particles were recorded on 16 mm ciné film using a Bolex reflex camera and a Hycam high speed camera. A scale was photographed prior to each run to provide a frame of reference. For systems where the resolution was poor, minimal amounts of a "biological oil red stain" were used to dye the dispersed fluid. Fluid properties were not measurably affected by the dye. Most of the photographs relied upon back-lighting, with flood lights illuminating a translucent white sheet of paper against which the drop appeared as a silhouette.

Further details of the experimental apparatus and procedures are available elsewhere (Wairegi 1972, 1974).

EXPERIMENTAL OBSERVATIONS

When large drops and bubbles moved freely under the influence of gravity, the following types of motion and shapes were observed:

(a) Rectilinear vertical motion of cap-shaped particles parallel to an axis of symmetry. In many cases, these drops or bubbles trailed thin "skirts" of the dispersed phase similar to those noted by Guthrie and Bradshaw (1969) for bubbles.

(b) Cap-shaped particles with unbalanced skirts or exfoliating continuously and asymmetrically from the rear.

(c) Crescent-shaped drops showing steady rectilinear motion.

(d) Biconcave disks showing steady rectilinear motion.

(e) Toroidal drops showing unsteady motion and break-up.

(f) Stretching, rolling and random wobbling motion accompanied by irregular shapes.

These shapes and types of motion will be discussed in turn, with particular attention devoted to (a). A ciné film has been prepared by the authors showing examples of the different types of motion, and this film may be loaned upon request. Some of the shapes observed are shown in figures 1 and 2.

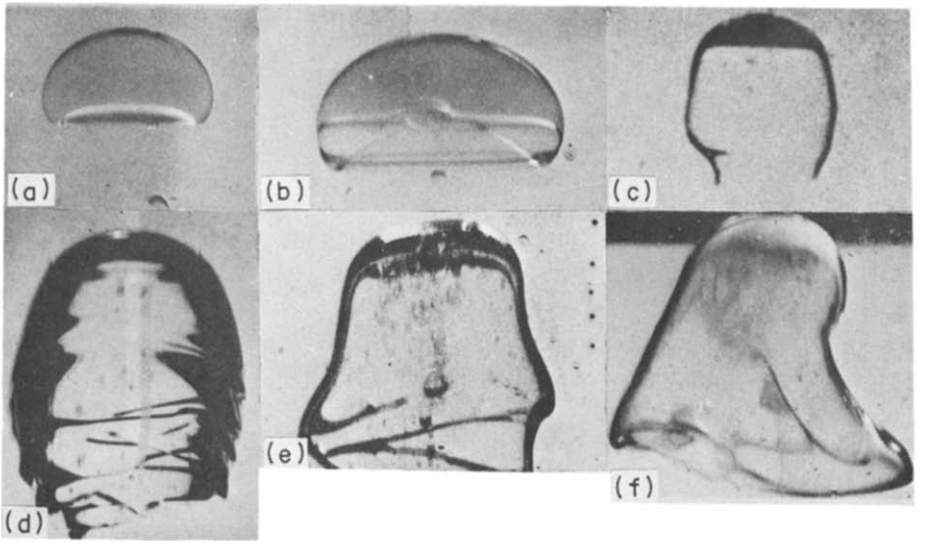

Figure 1. Shapes of ellipsoidal-cap drops with and without trailing skirts: (a) System 20, $d_e = 5.1$ cm; (b) System 20, $d_e = 6.8$ cm; (c) System 3, $d_e = 8.8$ cm; (d) System 11, $d_e = 5.8$ cm; (e) System 21, $d_e = 6.0$ cm; (f) System 22, $d_e = 6.4$ cm.

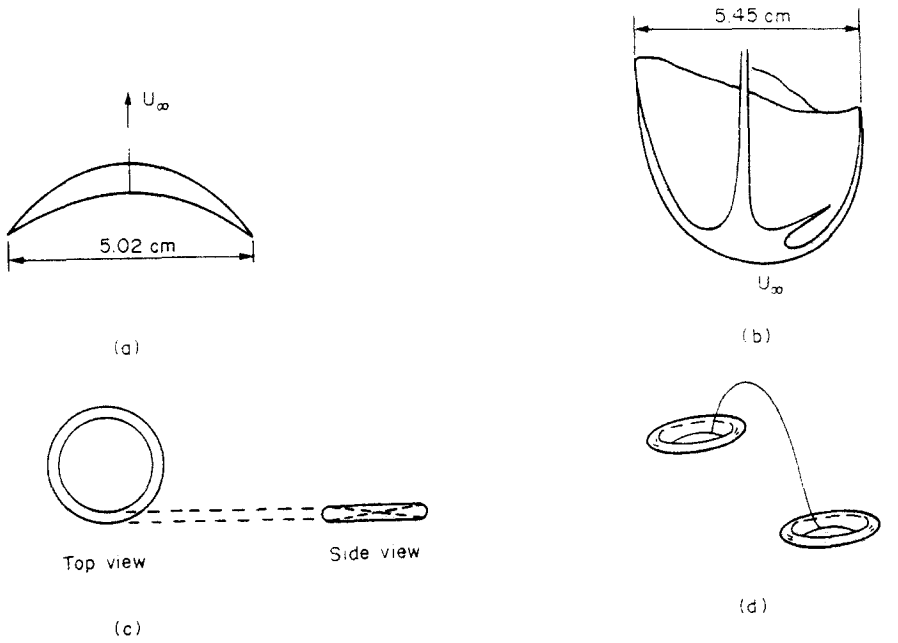

Figure 2. Other observed shapes of large liquid drops: (a) Crescent shape, System 7, $d_e = 3.7$ cm; (b) Exfoliating crescent. System 19, $d_e = 4.0$ cm; (c) Biconcave disk, System 17, $d_e = 1.1$ cm; (d) Toroids, System 18, $d_e \approx 1.5$ cm for original toroid.

(a) *Cap-shaped fluid particles*

"Spherical-capped" bubbles have received considerable attention in the literature due to their importance in fluidized beds, underwater explosions and metallurgical processes. For a review see Wegener & Parlange (1973). Similar shapes have been observed by Fararoui & Kinter (1961) and Shoemaker & Chazal (1969) for liquid–liquid systems, but very little data is available.

In the present work it was found that drops with Re greater than about 1.2 and Eo greater than 40 formed shapes that might loosely be termed spherical-caps, these criteria being the same as for spherical-cap gas bubbles (Grace 1973). However, the caps were more oblate spheroidal than spherical until $Re = \rho_c d_e U/\mu_c$ exceeded a value of approximately 40 at which point a circular arc could be fitted over the front 60° of the surface with no appreciable deviation. Here U is the terminal velocity of the fluid particle.

The terminal velocity of spherical-capped bubbles is predicted quite closely (Davenport *et al.* 1967) by a well-known equation developed by Davies & Taylor (1950):

$$U_B = \frac{2}{3}(gR)^{1/2}. \qquad [1]$$

In deriving this equation, it is assumed that the upper surface in the neighbourhood of the nose is perfectly spherical and of radius R and that the pressure distribution there can be calculated assuming irrotational flow past a complete sphere of radius R. Collins (1966) obtained a second improved approximation using a perturbation technique, but [1] is generally used because of its simplicity and the fact that the second approximation differs only slightly from the Davies and Taylor result.

The above equation was modified by Harrison *et al.* (1961) to account for cases where the dispersed phase density is of the same order as the continuous phase density. The resulting equation,

$$U = \frac{2}{3}(gR\Delta\rho/\rho_c)^{1/2} \qquad [2]$$

was obtained by assuming the dispersed fluid to be perfectly stagnant. In view of the oblate ellipsoidal-cap profile of drops in the range $1.2 < Re < 40$ ($Eo \geq 40$), we have developed an equation using essentially the Davies and Taylor assumptions, but with the pressure distribution derived assuming the cap is a portion of an oblate ellipsoid of revolution. The result is

$$U = E\sqrt{(gb\,\Delta\rho/\rho_c)} \qquad [3]$$

where b is the minor (vertical) semi-axis of the cap and

$$E = \frac{1}{e^3}[\sin^{-1} e - e\sqrt{(1-e^2)}] \qquad [4]$$

is a function only of the cap eccentricity, e. Since the derivation of the equation follows closely that given by Grace & Harrison (1967) for prolate ellipsoid-cap bubbles, only a brief outline has been given and this appears in the appendix. It is necessary, however, to say something about the appearance of the $\Delta\rho/\rho_c$ term in [3].

For all of the cases of ellipsoidal- or spherical-cap drops observed in the present work, the Reynolds number which characterizes the internal fluid motion, i.e. $Re_d = \rho_d d_e U/\mu_d$, was of order 10^2 or more even when $Re = \rho_c d_e U/\mu_d$ was of order unity. Hence it is reasonable to think in terms of a thin interior boundary layer (Harper & Moore 1968) across which the pressure is impressed by the slowly moving interior fluid. It is not necessary to assume that the interior fluid is completely stagnant (in violation of the no slip condition at the surface), but only that the bulk of the interior fluid is moving considerably slower than U relative to axes fixed on the drop. This has been confirmed by measurements of internal circulation (Wairegi 1974). Therefore the pressure impressed on the interior boundary layer is essentially the hydrostatic pressure distribution. With this assumption the $\Delta\rho/\rho_c$ term appears in [3] as shown in the appendix. Note that $E \to 2/3$ and $b \to R$ as $e \to 0$ so that [3] reduces to [2] as the ellipsoidal-cap becomes a spherical-cap; with the further simplication $\rho_c \ll \rho_d$, [2] and [3] reduce to [1]. The relationship between drop or bubble shape and M and Eo is considered elsewhere (Grace *et al.* 1976).

A comparison between predictions from [3] and [4] and experimentally measured values of U is given in figure 3 for $Eo \geq 40$ and $Re > 4$. Agreement is shown to be very favourable. The scatter in the data is characteristic of measurements for terminal velocities of bubbles and drops. Values of e to be used in testing the predictions were obtained from photographs of the drops by a procedure analogous to that described by Grace & Harrison (1967); i.e. a family of curves was drawn for different values of e for fixed values of cap aspect ratio, h/l where h and l are the height and half-width as shown in figure 4. A photographic image of the bubble or drop was then projected onto the diagram for the correct h/l ratio, and e was chosen visually. Values of e measured in this manner lay between 0 and 0.4. Further details are given by Wairegi (1972, 1974). Velocities obtained in the cylindrical column were corrected for wall effects by applying the correction factor suggested by Strom & Kintner (1958). However, this correction never exceeded 12% and was therefore not critical.

To summarize, [3] and [4] give a good prediction of the terminal velocities of ellipsoidal- and spherical-cap drops and bubbles for which $Eo \geq 40$ and $Re \geq 4$. For $Re \geq 40$ (with Eo still ≥ 40), e is very nearly 0 and it is more convenient to use [2] in place of [3] and [4]. The equations were found to apply whether or not the drops or bubbles were trailing skirts, thereby confirming one of the central assumptions of the theory, i.e. that the terminal velocity can be determined considering only the shape and motion in the frontal (nose) region.

(b) *Drops and bubbles with unbalanced or exfoliating skirts*

As indicated above, many of the drops studied in the present work trailed "skirts". These skirts are of considerable interest and will be the subject of a future paper. For the present, it is

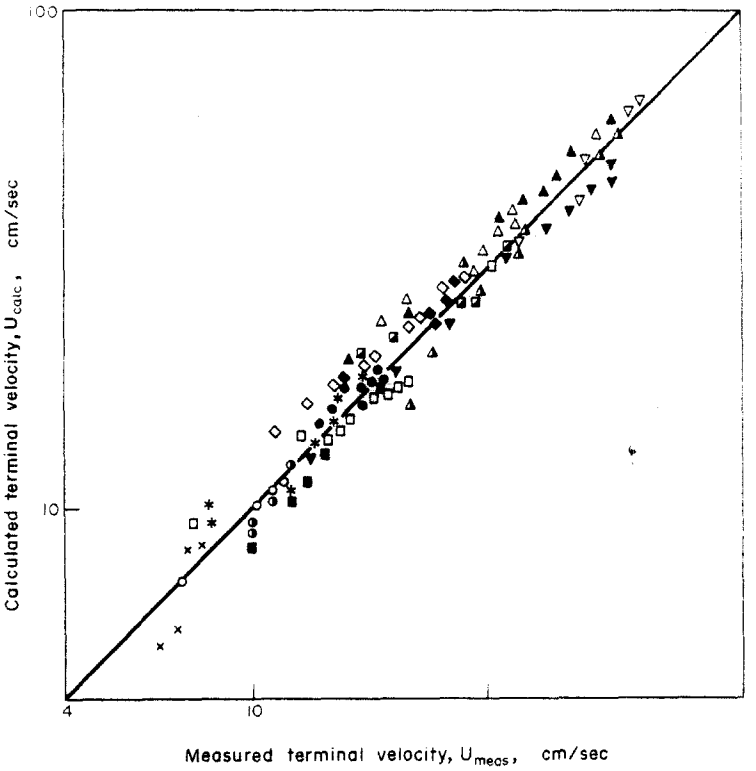

Figure 3. Comparison of terminal velocities predicted using [3] and [4] with experimental results for fifteen systems where $Eo \geq 40$ and $Re \geq 4$.

System	Symbol
1	●
2	◆
3	□
4	◇
5	▲
6	○
7	□
8	△
9	■
10	○
11	▼
10	▽
13	×
14	◭
16	*

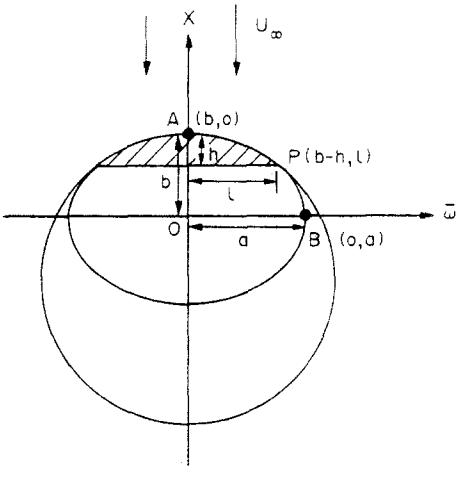

Figure 4. Definition sketch for an oblate spheroidal-cap drop or bubble.

worth noting that the skirts were not always of steady length or symmetrical. It was common to observe skirts growing and eventually becoming unbalanced (figure 1(c)), showing waves (figure 1(d)) and shedding from the rear (figures 1(e) and (f)). Similar observations were made by Wegener *et al.* (1971).

(c) *Crescent-shaped drops*

Unusual shapes occurred for large drops of silicone oil rising through a 3 *p* aqueous sugar solution (system 7) or falling through 2 *p* paraffin oil (system 19). Small drops were spherical, but as the size increased, a bulge developed at the front. The rear gradually became hollow while the front remained smooth and rounded giving rise finally to a crescent (quarter moon) shape (see figure 2(a)). As the size of the drops was increased still further, thin trailing elements developed at the outer rim. These filaments either broke into small droplets which were carried around in the wake or exfoliation occurred as shown in figure 2(b). Somewhat similar observations were made by Thomson & Newall (1885), but we have been unable to find any other report of crescent-shaped drops, i.e. drops where the rear surface is so deeply indented that it is nearly parallel to the curved front surface.

(d) *Biconcave disks*

Drops of silicone oil in ethylene glycol (system 17) in the range $1.0\text{ cm} < d_e < 1.6\text{ cm}$ assumed a steady shape resembling that of a red blood cell or a biconcave disk. A sketch is shown in figure 2(c). Larger drops became unstable and swayed in an irregular manner. A thickening appeared on one side while the opposite side thinned considerably. The indentations were observed to move around the drops as they rose through the column. As shown in table 2, terminal velocities of the biconcave drops show reasonable agreement with an equation developed by Levich (1962), i.e.

$$U = \left\{\frac{4\Delta\rho g\sigma}{\rho_c^2 C_D}\right\}^{1/4} \qquad [5]$$

where the drag coefficient C_D has been taken as unity.

(e) *Toroidal drops*

When a drop of glycerine ($1.5\text{ cm} < d_e < 2\text{ cm}$) was allowed to fall in paraffin oil (system 18), it descended as a toroid or vortex ring (figure 2(d)). As a drop travelled down the column, proturberances developed at a number of positions. The growing portions fell more quickly creating new toroids similar to the original. As the secondary toroids fell, they gave rise to still further toroids. As a result, a family of toroids soon appeared, each connected to neighbours by umbilical cords of the dispersed liquid. A similar phenomenon has been observed previously by Thomson & Newall (1885), Stuke (1954a, 1954b) and O'Brien (1961) for liquid pairs which are miscible, partially miscible and immiscible. Walters and Davidson (1963) also reported toroidal air bubbles (in water), but although the motion of these toroidal bubbles was unsteady, they did not proliferate in the manner described here for liquid toroids.

Table 2. Comparison of experimental terminal velocities of disk-shaped drops (system 17) with velocities calculated using [5]

Drop No.	Diameter d_e (cm)	Experimental terminal velocity (cm/s)	Terminal velocity obtained from [5] (cm/s)	Reynolds number *Re*
1	0.89	10.3	10.4	82.5
2	1.12	10.3	10.4	103.5
3	1.28	10.2	10.4	117.8
4	1.62	10.4	10.4	150.3

The number and size of toroids into which the original drop subdivided and their spacial distributions were quite irregular. As a result of the continuous breaking, the motion was highly unsteady and no meaningful data on velocities could be obtained, even using a high speed camera.

(f) *Stretching, rolling and random wobbling drops*

Drops of silicone oil rising through tap water (system 15) exhibited stretching, rolling and "random wobbling" (Schroeder 1964). It is notable that this behaviour occurs for low M systems, systems which have received extensive attention in previous work. Wobbling began to occur at a Reynolds number of about 200, a value which corresponds closely to the onset of vortex shedding behind rigid spheres. Thus the secondary motion of drops in low M systems is almost certainly associated with phenomena occurring in the wake.

DISCUSSION

The ellipsoidal-cap and spherical-cap liquid drops observed in the present work appear to be very similar to shapes observed for large gas bubbles and [2] and [3] apply under the same restrictions in either case. The same parallel appears to hold for the irregular wobbling shapes which occur in gas–liquid and in liquid–liquid systems for low M systems. However, there appears to be no strict gas–liquid analogue to the crescent and biconcave shapes and to the type of toroidal motion observed here for liquid drops. In all of these cases, the viscosity ratio, μ_d/μ_c was considerably higher than can generally be achieved when a gas is dispersed in a liquid and this may account for the peculiar shapes observed in systems 7, 17, 18 and 19 (see table 1).

The success of the Davies and Taylor theory (in extended form) for ellipsoidal- and spherical-cap liquid drops down to Reynolds numbers as low as 4 confirms the usefulness of the theory for large fluid particles. Levich's equation, [5], appears to work well for biconcave disk-shaped drops, but further confirmation with other systems is required. The other shapes observed are sufficiently complex or unstable that theoretical prediction of terminal velocities appears very difficult. The unstable shedding of the dispersed phase liquid from trailing skirts in some systems, while having negligible effect on terminal velocities for the length of column employed in the present study, must have a considerable influence on interphase transfer phenomena and deserves further study.

CONCLUSIONS

The most common shape of large fluid drop observed in the present study was the oblate ellipsoidal-cap or spherical-cap shape, the ellipsoidal-cap form being preferred at Reynolds numbers between about 1.2 and 40 and the spherical-cap form at higher Reynolds numbers. The terminal velocity for these drops is well predicted by an extended form of the Davies and Taylor theory and is independent of the occurrence of skirts, even growing or shredding skirts, at the rear.

Other shapes identified include crescent shapes, biconcave disks, toroids, and irregular wobbling shapes. The two latter shapes have been discussed previously in the literature, but the other two shapes appear to be previously unreported.

Acknowledgement—Financial assistance from the National Research Council of Canada is gratefully acknowledged.

REFERENCES

COLLINS, R. 1966 A second approximation for the velocity of a large gas bubble rising in an infinite liquid. *J. Fluid Mech.* **25**, 469–480.

DAVENPORT, W. G., RICHARDSON, F. D. & BRADSHAW, A. V. 1967 Spheridal cap bubbles in low density liquids. *Chem. Engng Sci.* **22**, 1221–1235.

DAVIES, R. M. & TAYLOR, G. I. 1950 The mechanics of large bubbles rising through extended liquids and through liquids in tubes. *Proc. R. Soc.* **A200**, 375–390.

FARAROUI, A. & KINTER, R. C. 1961 Flow and shape of drops in non-Newtonian fluids. *Trans. Soc. Rheol.* **5**, 369–380.

GRACE, J. R. 1973 Shapes and velocities of bubbles rising in infinite liquids. *Trans. Instn Chem. Engrs* **51**, 116–120.

GRACE, J. R. & HARRISON, D. 1967 The influence of bubble shape on the rising velocities of large bubbles. *Chem. Engng Sci.* **22**, 1337–1347.

GRACE, J. R., WAIREGI, T. & NGUYEN, T. H. 1976 Shapes and velocities of single drops and bubbles moving freely through immiscible liquids, *Trans. Instn. Chem. Engrs.*, to be published.

GUTHRIE, R. I. L. & BRADSHAW, A. V. 1969 The stability of gas envolopes trailed behind spherical cap bubbles rising through viscous liquids. *Chem. Engng Sci.* **24**, 913–917.

HARPER, J. F. & MOORE, D. W. 1968 The motion of spherical liquid drops at high Reynolds numbers. *J. Fluid Mech.* **32**, 367–391.

HARRISON, D., DAVIDSON, J. F. & DE KOCK, J. W. 1961 On the nature of aggregative fluidization. *Trans. Instn Chem. Engrs* **39**, 202–211.

LEVICH, V. G. 1962 *Physicochemical Hydrodynamics.* Prentice-Hall, New York.

MILNE-THOMSON, L. M. 1968 *Theoretical Hydrodynamics*, 5th Ed. Macmillan, London.

O'BRIEN, V. 1961 Why raindrops break up—vortex instability. *J. Met.* **18**, 549–552.

SCHROEDER, R. R. 1964 Oscillations of droplets falling in a liquid field. Ph.D. Thesis, Illinois Inst. of Technology.

SHOEMAKER, P. D. & CHAZAL, L. E. 1969 Dimpled and skirted liquid drops moving through viscous media. *Chem. Engng Sci.* **24**, 797–799.

STROM, J. R. & KINTNER, R. C. 1958 Wall effect for the fall of single drops. *A.I.Ch.E.Jl* **4**, 153–156.

STUKE, B. 1954a Zur Bildung von Wirbelringen. *Z. Phys.* **137**, 376–379.

STUKE, B. 1954b Die Bewegung von Gasblasen und Flüssigkeitstropfen. *Umschau* **54**, 715–717.

THOMSON, J. J. & NEWALL, H. P. 1885 On the deformation and drag of a falling viscous drop at low Reynolds number. *Proc. R. Soc.* **39**, 466–487.

WAIREGI, T. 1972 The behaviour of dimpled drops. M. Eng. Thesis, McGill University.

WAIREGI, T. 1974 The mechanics of large bubbles and drops moving through extended liquid media. Ph.D. Thesis, McGill University.

WALTERS, J. K. & DAVIDSON, J. F. 1963 The initial motion of a gas bubble formed in an inviscid liquid. *J. Fluid Mech.* **17**, 321–336.

WEGENER, P. P. & PARLANGE, J. Y. 1973 Spherical-cap bubbles, *Ann. Rev. Fluid Mech.* **5**, 79–100.

WEGENER, P. P., SUNDELL, R. E. & PARLANGE, J. Y. 1971 Spherical-cap bubbles rising in liquids. *Z. Flugwiss.* **19**, 347–352.

APPENDIX

Terminal Velocity of Oblate Ellipsoidal-Capped Drop

We assume that the terminal velocity of a (large) ellipsoidal-capped drop may be determined by balancing pressure terms over the nose region in a manner analogous to the Davies & Taylor (1950) treatment for spherical-cap bubbles. Thus the effect of wakes and of trailing skirts (if any) are neglected. The flow is assumed axisymmetric and steady relative to axes fixed on the drop. Interfacial tension forces are ignored and the pressure over the front region is calculated from potential flow theory assuming a complete oblate spheroid.

The stream function for an oblate spheroid moving along its axis of symmetry at velocity U is given by Milne-Thomson (1968). By superimposing a uniform stream of velocity U in the opposite direction we obtain the stream function for streaming past an oblate ellipsoid of revolution, i.e.

$$\psi = -\frac{Uc^2}{2K}\sin^2\eta\{K\cosh^2\xi - (\sinh\xi - \cosh^2\xi\cot^{-1}\sinh\xi)\} \qquad [A1]$$

where c is the focal length of the ellipse, η and ξ are elliptical coordinates and

$$K = \sin^{-1} e - e\sqrt{(1-e^2)}. \quad [A2]$$

The surface velocity is given by

$$q_0 = \frac{1}{J\bar{\omega}} \frac{\partial \psi}{\partial \xi}\bigg|_{\xi=\xi_0} \quad [A3]$$

where ξ_0 is the value of ξ at the surface, $\bar{\omega}$ is a Cartesian coordinate and

$$J^2 = f'(z)\bar{f}'(\bar{z}) \quad [A4]$$

with $f(z)$ the conformal transformation function defined by Milne-Thomson (1968).

After substitution and considerable simplification, we obtain

$$q_0 = \frac{Ue^3 \sin \eta}{K\{(1-e^2)\sin^2 \eta + \cos^2 \eta\}^{1/2}}. \quad [A5]$$

Applying Bernoulli's theorem between the front stagnation point and another point on the surface of the drop, we obtain the surface pressure as

$$p = p_s + \rho_c g b(1-\cos \eta) - \rho_c q_0^2/2 \quad [A6]$$

where p_s is the pressure at the front stagnation point. If we assume that the interior pressure distribution is simply the hydrostatic pressure distribution for the dispersed fluid as discussed above, then p must also be given by

$$p = p_s + \rho_d g b(1-\cos \eta). \quad [A7]$$

Combination of [A6] and [A7] and rearrangement yields

$$U^2 = 2gb\frac{\Delta\rho}{\rho_c}\frac{K^2}{e^6}\left(\frac{1-\cos \eta}{\sin^2 \eta}\right)[(1-e^2)\sin^2 \eta + \cos^2 \eta] \quad [A8]$$

where

$$\Delta\rho = |\rho_c - \rho_d|. \quad [A9]$$

Table 3. Variation of velocity coefficient E with eccentricity e

Eccentricity e	E
0.0	0.667
0.1	0.669
0.2	0.675
0.3	0.686
0.4	0.702
0.5	0.725
0.6	0.757
0.7	0.803
0.8	0.874
0.9	0.998
1.0	1.571

We require that [A8] be satisfied in the limit as $\eta \to 0$ and this leads to an expression for the drop terminal velocity, i.e.

$$U = E\sqrt{(gb\Delta\rho/\rho_c)} \qquad [A10]$$

where $E = K/e^3$. It may be shown (Wairegi 1972) that $E = 2/3$ for the limiting case where $e = 0$ for spherical-cap drops. Values of E are tabulated in table 3 for different values of e.